INTERNATIONAL JOURNAL FOR NUMERICAL METHODS IN FLUIDS
Int. J. Numer. Meth. Fluids 2005; **47**:979–985
Published online 20 January 2005 in Wiley InterScience (www.interscience.wiley.com). DOI: 10.1002/fld.924

A new symmetry-preserving Cartesian-grid method for computing flow past arbitrarily shaped objects

Marc Dröge and Roel Verstappen*,†

Research Institute of Mathematics and Computing Science, University of Groningen, The Netherlands

SUMMARY

This paper deals with a numerical method for solving the unsteady, incompressible Navier–Stokes equations in domains of arbitrarily shaped boundaries, where the boundary is represented using the Cartesian-grid approach. We introduce a novel cut-cell discretization, which preserves the symmetry of convection and diffusion. That is, convection is discretized by a skew-symmetric operator and diffusion is approximated by a symmetric, positive-definite coefficient matrix. The resulting semi-discrete (continuous in time) system conserves the kinetic energy if the dissipation is turned off; the energy decreases if dissipation is turned on. The method is successfully tested for an incompressible, unsteady flow around a circular cylinder at $Re = 100$. Copyright © 2005 John Wiley & Sons, Ltd.

KEY WORDS: Cartesian-grid method; symmetry-preserving discretization; flow past bluff body

1. INTRODUCTION

Many problems in computational fluid dynamics have domains with complicated boundaries. These problems can be dealt with in three different ways. Classified by the type of grid that is used, the three approaches are called boundary-fitted structured, boundary-fitted unstructured, or Cartesian. This paper treats the Cartesian-grid method (see e.g. References [1–4]) for computing a fluid flow governed by unsteady, incompressible Navier–Stokes equations. The discretization of fluxes through the irregularly shaped cell faces created by the intersection of the boundary with the Cartesian grid forms the primary difficulty. Away from the boundary, the simple structure of the Cartesian grid allows to retain much of the numerical techniques that have proven to be successful for flows in simple, grid-aligned domains. For such flows, we have proposed to compute numerical solutions of the Navier–Stokes equations in such a manner that the difference operators do have the same symmetry properties as the corresponding differential operators [5]. Applied to the incompressible

*Correspondence to: Roel Verstappen, Research Institute of Mathematics and Computing Science, University of Groningen, P.O. Box 800, 9700 AV Groningen, The Netherlands.
†E-mail: verstappen@math.rug.nl

Received 27 April 2004
Revised 15 December 2004
Accepted 15 December 2004

Navier–Stokes equations, the symmetry-preserving discretization method yields a dynamical system of the form

$$\mathbf{\Omega}\frac{\mathrm{d}\mathbf{u}_h}{\mathrm{d}t} + \mathbf{C}(\mathbf{u}_h)\mathbf{u}_h + \mathbf{D}\mathbf{u}_h - \mathbf{M}^*\mathbf{p}_h = \mathbf{0} \quad \mathbf{M}\mathbf{u}_h = \mathbf{0} \tag{1}$$

in which the convective coefficient matrix $\mathbf{C}(\mathbf{u}_h)$ is skew symmetric like the underlying differential operator $(\mathbf{u}\cdot\nabla)$, i.e.

$$\mathbf{C}(\mathbf{u}_h) + \mathbf{C}(\mathbf{u}_h)^* = \mathbf{0} \tag{2}$$

and the discrete diffusive operator $\mathbf{D}$ is symmetric, positive definite like $-\nabla^2$. Here, $\mathbf{u}_h$ denotes the semi-discrete velocity vector, $\mathbf{p}_h$ stands for the discrete pressure, $\mathbf{\Omega}$ is a (positive definite) diagonal matrix representing the sizes of the control volumes; $\mathbf{M}$ is the coefficient matrix of the discretization of the integral form of the law of conservation of mass.

Mimicking crucial properties of differential operators forms in itself a motivation for discretizing them in a certain manner. We give it a concrete form by noting that the energy $||\mathbf{u}_h||^2 = \mathbf{u}_h^*\mathbf{\Omega}\mathbf{u}_h$ of any solution of (1)–(2) evolves according to

$$\frac{\mathrm{d}}{\mathrm{d}t}(\mathbf{u}_h^*\mathbf{\Omega}\mathbf{u}_h) \overset{(1)}{=} -\mathbf{u}_h^*(\mathbf{C}(\mathbf{u}_h) + \mathbf{C}(\mathbf{u}_h)^*)\mathbf{u}_h - \mathbf{u}_h^*(\mathbf{D} + \mathbf{D}^*)\mathbf{u}_h \overset{(2)}{=} -\mathbf{u}_h^*(\mathbf{D} + \mathbf{D}^*)\mathbf{u}_h$$

where the right-hand side is negative for all $\mathbf{u}_h \neq \mathbf{0}$ since $\mathbf{D}$ is a symmetric, positive-definite matrix. This implies that the semi-discrete system (1) is stable. So, in conclusion, if $\mathbf{C}(\mathbf{u}_h)$ is skew symmetric and $\mathbf{D}$ positive definite, a solution of (1) can be obtained on any grid. Note that the discrete pressure does not contribute to the evolution of the discrete energy because $(\mathbf{M}^*\mathbf{p}_h)^*\mathbf{u}_h = \mathbf{p}_h^*\mathbf{M}\mathbf{u}_h = 0$. More details can be found in References [5–7] and the references therein.

In this paper, the symmetry-preserving discretization method is generalized to a Cartesian-grid method with cut cells for representing arbitrarily shaped domains. That is, the convective flux through irregularly shaped boundary cells is discretized such that the associated coefficient matrix $\mathbf{C}(\mathbf{u}_h)$ is skew symmetric and the diffusive matrix is symmetric, positive definite. The method is tested for a convective flow in a skew channel as well as for an unsteady viscous flow around a circular cylinder.

2. SYMMETRY-PRESERVING DISCRETIZATION

Various ways exist to discretize convective and diffusive fluxes through cut cells. In this section, we will discuss a finite-volume discretization that preserves the symmetry.

We assume that the geometry is so well resolved on the grid that the boundary of the geometry can be approximated linearly in any cut cell. The part of the grid cell $[x_{i-1}, x_i] \times [y_{j-1}, y_j]$ that is open to fluid flow is denoted by $\Omega_{i,j}$. The discrete velocity $(u_{i,j}, v_{i,j})$ is staggered. The control volume for $u_{i,j}$ takes up the right half of $\Omega_{i,j}$ and the left half of $\Omega_{i+1,j}$. This choice is illustrated in Figure 1 by means of three examples. The control volume for $v_{i,j}$ is defined in the same manner: its definition can be obtained from that of $u_{i,j}$ by exchanging x and y. For uncut cells, the control volumes are identical to those in Reference [8].

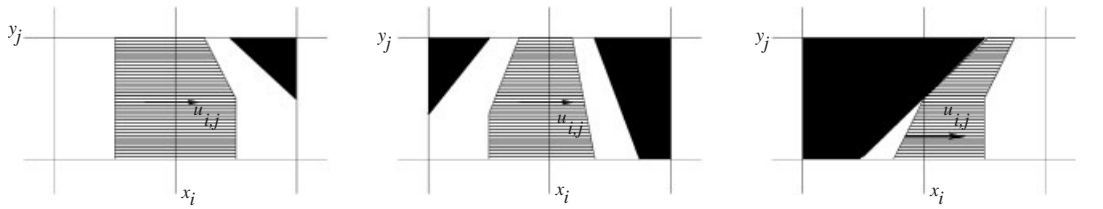

Figure 1. Three control volumes for $u_{i,j}$. The parts that are not open to flow are coloured black.

When the normal velocity vanishes at the boundary of the geometry, incompressibility states that the integral of the normal velocity over the surface of any grid cell $[x_{i-1}, x_i] \times [y_{j-1}, y_j]$ is zero:

$$\overline{u}_{i,j} + \overline{v}_{i,j} - \overline{u}_{i-1,j} - \overline{v}_{i,j-1} = 0 \tag{3}$$

where the mass fluxes through the grid faces are defined by

$$\overline{u}_{i,j} = \int_{y_{j-1}}^{y_j} u(x_i, y, t)\delta(x_i, y)\,\mathrm{d}y \quad \text{and} \quad \overline{v}_{i,j} = \int_{x_{i-1}}^{x_i} v(x, y_j, t)\delta(x, y_j)\,\mathrm{d}x \tag{4}$$

in which the fluid domain is indicated by a function $\delta(x, y)$, that equals one inside the fluid and zero outside. Note, the combination (3)–(4) does not yet contain a discretization error.

As mass and momentum are transported at equal velocity, we will use (4) to describe the velocity at which momentum is transported. To start, the momentum flux through a surface S is approximated by

$$\int_S u\mathbf{u}\cdot\mathbf{n}\,\mathrm{d}S \approx u_S \int_S \mathbf{u}\cdot\mathbf{n}\,\mathrm{d}S$$

where u_S denotes a characteristic value of u at the surface S. Thus, the transport of momentum through the faces of a control volume for $u_{i,j}$ becomes

$$|\Omega_{i+1/2,j}|\,\frac{\mathrm{d}u_{i,j}}{\mathrm{d}t} + u_{i+1/2,j}\overline{u}_{ni+1/2,j} + u_{i,j+1/2}\overline{v}_{i+1/2,j} - u_{i-1/2,j}\overline{u}_{ni-1/2,j} - u_{i,j-1/2}\overline{v}_{i+1/2,j-1} \tag{5}$$

where $|\Omega_{i+1/2,j}|$ denotes the size of the control volume for $u_{i,j}$. The non-integer indices in (5) refer to the faces of the cell for $u_{i,j}$. For example, $u_{i+1/2,j}$ stands for a characteristic u-velocity at the interface between the cells for $u_{i,j}$ and $u_{i+1,j}$, and $\overline{v}_{i+1/2,j}$ denotes the mass flux through the common boundary of the control volumes for $u_{i,j}$ and $u_{i,j+1}$, etc. As can be seen in Figure 2 (left), the mass flux through a part of the interface between the control volumes for $u_{i,j}$ and $u_{i+1,j}$ need not be aligned with u. Therefore, it is denoted by $\overline{u}_n$ and not by $\overline{u}$.

The skew symmetry of the convective operator determines the interpolation rule for both the velocity and mass flux at the control faces. To illustrate this, we consider the general rule

$$u_{i+1/2,j} = (1 - \alpha_{i,j})u_{i+1,j} + \alpha_{i,j}u_{i,j} \quad \text{and} \quad u_{i,j+1/2} = (1 - \beta_{i,j})u_{i,j+1} + \beta_{i,j}u_{i,j} \tag{6}$$

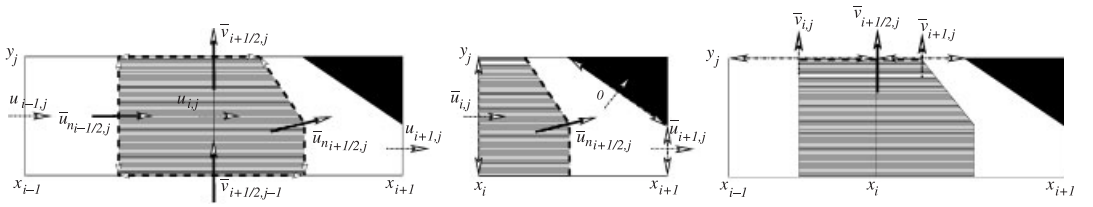

Figure 2. Mass flux through the boundary of the control volume for $u_{i,j}$ (left-hand side). The middle figure illustrates the interpolation of the mass flux $\overline{u}_{ni+1/2,j}$; the right-hand side shows $\overline{v}_{i+1/2,j}$. The black triangle is not open to flow. The dashed line represents the control face.

and conceive Equation (5) together with the interpolation rule (6) as an expression for the velocities, where the mass fluxes form the coefficients. Thus, we can write the discretization (5)+(6), together with an analogous set for the v-component, in matrix–vector notation as

$$\mathbf{\Omega}\frac{\mathrm{d}\mathbf{u}_h}{\mathrm{d}t} + \mathbf{C}(\bar{\mathbf{u}})\mathbf{u}_h$$

where the coefficient matrix $\mathbf{C}(\bar{\mathbf{u}})$ depends on the mass fluxes through the control faces and the weights in the interpolation rule. In the introductory section, we saw that (for $\mathbf{D}=\mathbf{0}$) the spatial discretization (1) conserves the energy $\mathbf{u}_h^*\mathbf{\Omega}\mathbf{u}_h$ if and only if the convective coefficient matrix $\mathbf{C}(\bar{\mathbf{u}})$ is skew symmetric. This condition determines the weights $\alpha_{i,j}$ and $\beta_{i,j}$ in (6). Indeed, the matrix $\mathbf{C}(\bar{\mathbf{u}}) - \mathrm{diag}(\mathbf{C}(\bar{\mathbf{u}}))$ is skew symmetric if and only if the weights in the interpolation (6) are equal to the uniform weights $\alpha_{i,j}=1/2$ and $\beta_{i,j}=1/2$. To make $\mathbf{C}(\bar{\mathbf{u}})$ skew symmetric, the interpolation rule for $\overline{u}$ and $\overline{v}$ is determined by the requirement that the diagonal has to be zero. By substituting (6) into (5), we see that the diagonal entries are zero if and only if (mass is conserved, that is (3) holds, and) the mass fluxes in (5) are interpolated to the control faces with constant weights one half:

$$\overline{u}_{ni+1/2,j} = \tfrac{1}{2}(\overline{u}_{i+1,j} + \overline{u}_{i,j}) \quad \text{and} \quad \overline{v}_{i+1/2,j} = \tfrac{1}{2}(\overline{v}_{i+1,j} + \overline{v}_{i,j}) \tag{7}$$

The interpolation of $\overline{u}_{ni+1/2,j}$ is illustrated in Figure 2 (middle). The mass flux $\overline{u}_{ni+1/2,j}$ through the right-hand face of the control volume for $u_{i,j}$ is written as the average of the mass flux at both sides: $\overline{u}_{ni+1/2,j} = \frac{1}{2}(\overline{u}_{\mathrm{left}} + \overline{u}_{\mathrm{right}})$, where we take the flux through the face $x=x_i$ for the left-hand side, that is $\overline{u}_{\mathrm{left}} = \overline{u}_{i,j}$. The right-hand contribution is approximated by the sum of the mass flux through the hypotenuse of the triangle that is not open to the flow and the mass flux through the open part of the face $x=x_{i+1}$, i.e. $\overline{u}_{\mathrm{right}} = 0 + \overline{u}_{i+1,j}$. The flux $\overline{v}_{i+1/2,j}$ is also seen as the sum of a left- and right-hand contribution, $\overline{v}_{i+1/2,j} = \overline{v}_{\mathrm{left}} + \overline{v}_{\mathrm{right}}$, with $\overline{v}_{\mathrm{left}} = \frac{1}{2}\overline{v}_{i,j}$ and $\overline{v}_{\mathrm{right}} = \frac{1}{2}\overline{v}_{i+1,j}$, see Figure 2 (right).

Obviously, the mass flux $\bar{\mathbf{u}}$ needs to be expressed in terms of the discrete velocity vector $\mathbf{u}_h$ to close the discretization. The coefficient matrix $\mathbf{C}(\bar{\mathbf{u}})$ becomes a function of the discrete velocity $\mathbf{u}_h$ then $\mathbf{C}(\mathbf{u}_h) = \mathbf{C}(\bar{\mathbf{u}}(\mathbf{u}_h))$. The matrix $\mathbf{C}(\mathbf{u}_h)$ is skew symmetric for any relation between $\bar{\mathbf{u}}$ and $\mathbf{u}_h$. We relate the mass fluxes $\bar{\mathbf{u}}$ to the discrete velocity $\mathbf{u}_h$ by means of

$$\overline{u}_{i,j} = u_{i,j}\int_{y_{j-1}}^{y_j} \delta(x_i, y)\,\mathrm{d}y \quad \text{and} \quad \overline{v}_{i,j} = v_{i,j}\int_{x_{i-1}}^{x_i} \delta(x, y_j)\,\mathrm{d}x \tag{8}$$

Substituting these approximations into Equation (3) gives the discrete continuity constraint, which confines the discrete velocity to $\mathbf{M}\mathbf{u}_h = \mathbf{0}$.

In order to incorporate the free-slip condition in cut cells, we set all virtual, out-of-domain velocities that occur in (6) equal to zero first. The resulting discretization, say $\mathbf{C}(\bar{\mathbf{u}})\mathbf{u}_h$, is corrected in cut cells by subtracting $\mathbf{C}(\bar{\mathbf{u}}^{\text{lin}})\mathbf{u}_h^{\text{lin}}$, where (in any cut cell) $\mathbf{u}^{\text{lin}}$ is zero in the wall-normal direction and is a linear function of the normal co-ordinate in the tangential direction. The coefficients of this linear function are determined such that $\mathbf{u}^{\text{lin}}$ fits the nearest-wall velocities of $\mathbf{u}_h$. Thus, the convective discretization is made exact for linear velocity profiles satisfying the free-slip condition.

In the continuous case the diffusion corresponds to a symmetric, positive-definite operator. We want this property to hold also for the discrete operator $\mathbf{D}$ in Equation (1). To that end, the diffusive flux through the interface S between the control volumes of $u_{i-1,j}$ and $u_{i,j}$ may be approximated in a common way

$$\frac{1}{Re}\int_S \nabla u \cdot \mathbf{n}\,\mathrm{d}s \approx \frac{u_{i-1,j} - u_{i,j}}{Re|\mathbf{n}_S|}|S| \tag{9}$$

where the length of the vector $\mathbf{n}_S$ is approximated in terms of the size of the face S and sizes of the control volumes for $u_{i-1,j}$ and $u_{i,j}$. The diffusive flux through the other faces of the control cell for $u_{i,j}$ is discretized similarly. The resulting coefficient matrix $\mathbf{D}$ is symmetric and positive definite.

The temporal discretization is carried out according to

$$\boldsymbol{\Omega}\frac{\mathbf{u}_h^{n+1} - \mathbf{u}_h^n}{\delta t} + (\mathbf{C}(\tfrac{3}{2}\mathbf{u}_h^n - \tfrac{1}{2}\mathbf{u}_h^{n-1}) + \mathbf{D})(\tfrac{3}{2}\mathbf{u}_h^n - \tfrac{1}{2}\mathbf{u}_h^{n-1}) - \mathbf{M}^*\mathbf{p}_h^{n+1} = \mathbf{0}, \quad \mathbf{M}\mathbf{u}_h^{n+1} = \mathbf{0}$$

where δt denotes the time step and the time level is indicated by the upper index. Here, the convective and diffusive term are integrated by means of a one-leg method. For details, the reader is referred to Section V.6 in Reference [9]. The pressure and incompressibility constraint are treated implicitly in time. The resulting linear system of equations for the discrete pressure is solved iteratively with the help of a modified incomplete Choleski conjugate gradient (MICCG) method [10].

3. RESULTS

The convective discretization is made exact for linear velocities satisfying the free-slip condition. To investigate the order of convergence of the convective discretization, we consider a quadratic velocity profile in a channel placed skewed to the grid (at an angle of 41° with the horizontal axis). Five simulations have been performed on grids varying from 32^2 to 512^2 cells. The width of the channel is covered by 2–32 cells, respectively. The mean error and the order of convergence are shown in Table I. As can be seen, the convective discretization is indeed second-order accurate.

Next, the Cartesian-grid method is applied to compute the unsteady, viscous flow around a circular cylinder at $Re = 100$, where the Reynolds number Re is based upon the diameter of the cylinder and the free stream velocity. This flow has served as a test case for various

Table I. Convergence upon grid refinement; skew channel.

Number of grid cells	Cells in channel width	Mean error	Order of convergence
512^2	32	0.12×10^{-4}	1.9
256^2	16	0.45×10^{-4}	1.9
128^2	8	1.75×10^{-4}	2.0
64^2	4	6.88×10^{-4}	1.9
32^2	2	25×10^{-4}	

Table II. Comparison with other simulations and experiments. When given, the drag coefficient is written as the sum of the pressure drag and the viscous drag. The experimental data are taken from [13] and the references therein.

	St	$C_{D,p}$	$C_{D,\mathrm{vis}}$	C_D	max C_L	θ_{sep}
Present	0.165	0.93	0.31	1.24	0.30	117
Reference [11]	0.164	0.97	0.34	1.31	0.314	117.4
Reference [12]	0.165			1.253	0.38	113.5
Experiments	0.164–0.165			1.24–1.26		

numerical approaches. We will compare our results with those in References [11–13]. Kravchenko *et al.* [11] considered the flow past a circular cylinder to evaluate their Galerkin B-spline method. Persillon and Braza [12] studied the test case by means of a second-order, curvilinear, finite-volume method. Experimental data can be found in Reference [13] and the references therein.

To confine the flow domain, fictitious boundaries are necessary (sufficiently) far away from the cylinder. We take the inflow boundary at four diameters upstream from the cylinder. The inflow condition reads $u = 1$, $v = 0$. The lateral boundaries are taken 8 diameters apart. At these boundaries the normal derivatives of the components of the velocity are set equal to zero. The outflow is located at 10 diameters past the cylinder. Also at the outflow, Neumann conditions are applied. Computations have been performed on four grids consisting of 100×120, 150×180, 200×240 and 400×480 points (in lateral and streamwise direction), respectively. The time step is taken equal to 1.25×10^{-3} for the finest grid and 5×10^{-3} for the other grids.

Table II shows a comparison of bulk quantities as obtained from our fine-grid simulation with those of the references mentioned above. The good agreement with the other numerical simulation techniques as well as with the physical experiments confirms the correct behaviour of the present approach and shows that the symmetry-preserving Cartesian-grid method forms a good alternative for boundary-fitted structured and boundary-fitted unstructured methods.

Figure 3 (left) displays the pressure distribution at the surface of the cylinder as obtained with the symmetry-preserving Cartesian-grid method. At all four grids the numerical result is in good agreement with an experimentally determined pressure distribution. To study the convergence of the symmetry-preserving scheme upon grid refinement, the pressure drag $C_{D,p}$

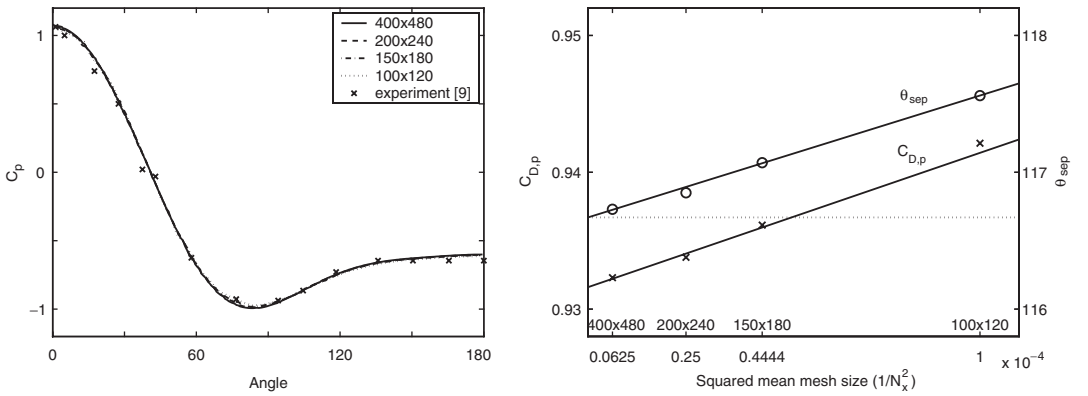

Figure 3. A comparison between experiment and simulation: the pressure distribution at the surface of the cylinder, as function of the angle (left). The separation angle Θ_{sep} and pressure drag $C_{D,p}$ as function of the square of the mean mesh size (right).

and the separation angle Θ_{sep} are shown as functions of the square of the mean mesh size in Figure 3 (right). The figure shows that $C_{D,p}$ and Θ_{sep} are (approximately) linear functions of the square of the mean mesh size. Hence, we may conclude that the scheme is second order.

REFERENCES

1. Purvis J, Burkhalter J. Prediction of critical Mach number store configurations. *AIAA Journal* 1979; **17**: 1170–1177.
2. Berger M, LeVeque R. An adaptive Cartesian mesh algorithm for the Euler equations in arbitrary geometries. *Proceedings of the 9th AIAA CFD Conference*, Buffalo, NY, 1991; 1–7.
3. Ye T, Mittal R, Udaykumar HS, Shyy W. An accurate Cartesian grid method for viscous incompressible flow with complex boundaries. *Journal of Computational Physics* 1999; **156**:209–240.
4. Calhoun D, LeVeque RJ. A Cartesian grid finite volume method for the advection–diffusion equation in irregular geometries. *Journal of Computational Physics* 2000; **157**:143–180.
5. Verstappen RWCP, Veldman AEP. Symmetry-preserving discretization of turbulent flow. *Journal of Computational Physics* 2003; **187**:343–368.
6. Morinishi Y, Lund TS, Vasilyev OV, Moin P. Fully conservative higher order finite difference schemes for incompressible flow. *Journal of Computational Physics* 1998; **143**:90–124.
7. Ducros F, Laporte F, Soulères T, Guinot V, Moinat P, Caruelle B. High-order fluxes for conservative skew-symmetric-like schemes in structured meshes: application to compressible flows. *Journal of Computational Physics* 2000; **161**:114–139.
8. Harlow FH, Welsh JE. Numerical calculation of time-dependent viscous incompressible flow of fluid with free surface. *Physics of Fluids* 1965; **8**:2182–2189.
9. Hairer E, Wanner G. *Solving Ordinary Differential Equations II*. Springer: Berlin, 1991.
10. Gustavson I. A class of first-order factorization methods. *BIT* 1978; **18**:142–156.
11. Kravchenko AG, Moin P, Shariff K. B-Spline method and zonal grids for simulations of complex turbulent flows. *Journal of Computational Physics* 1999; **151**:757–789.
12. Persillon H, Braza M. Physical analysis of the transition to turbulence in the wake of a circular cylinder by three-dimensional Navier–Stokes simulation. *Journal of Fluid Mechanics* 1998; **365**:23–88.
13. Zdravkovich MM. *Flow Around Circular Cylinders. Volume 1: Fundamentals*. Oxford University Press: Oxford, 1997.

